HHS Public Access

Author manuscript

*Angew Chem Int Ed Engl*. Author manuscript; available in PMC 2022 March 08.

Published in final edited form as:

*Angew Chem Int Ed Engl*. 2021 March 08; 60(11): 5907–5912. doi:10.1002/anie.202013791.

# Ferric Heme Superoxide Reductive Transformations to Ferric Heme (Hydro)Peroxide Species: Spectroscopic Characterization and Thermodynamic Implications for H-atom Transfer (HAT)

**Hyun Kim**[a], **Patrick J. Rogler**[a], **Savita K. Sharma**[a], **Andrew W. Schaefer**[b], **Edward I. Solomon**[b], **Kenneth D. Karlin**[a]

[a]Chemistry Department, Johns Hopkins University, Baltimore, Maryland 21218, United States.

[b]Chemistry Department, Stanford University, Stanford, California 94305, United States.

## Abstract

A new end-on low-spin ferric heme peroxide, $[(P^{Im})Fe^{III}—(O_2^{2-})]^-$ (**$P^{Im}$-*P***), and subsequently formed hydroperoxide species, $[(P^{Im})Fe^{III}—(OOH)]$ (**$P^{Im}$-*HP***) are generated utilizing the iron-porphyrinate $P^{Im}$ with its tethered axial base imidazolyl group. Measured thermodynamic parameters, the ferric heme superoxide $[(P^{Im})Fe^{III}—(O_2^{\bullet-})]$ (**$P^{Im}$-*S***) reduction potential ($E°'$) and the **$P^{Im}$-*HP*** p$K_a$ value, lead to the finding of the OO—H bond dissociation free energy (BDFE) of **$P^{Im}$-*HP*** as 69.5 kcal/mol, using a thermodynamic square scheme and Bordwell relationship. The results are validated by the observed oxidizing ability of **$P^{Im}$-*S*** via hydrogen atom transfer (HAT) compared to that of the $F_8$ superoxide complex, $[(F_8)Fe^{III}—(O_2^{\bullet-})]$ (***S***) ($F_8$ = tetrakis(2,6-difluorophenyl)porphyrinate, without an internally appended axial base imidazolyl), as determined from reactivity comparison of superoxide complexes **$P^{Im}$-*S*** and ***S*** with the hydroxylamine (O—H) substrates TEMPO-H and ABNO-H.

Thermodynamic comparisons for $O_2$-derived iron-porphyrinate interrelated ferric heme superoxide, peroxide and hydroperoxide analogs in the presence and absence of an appended imidazolyl axial base are presented.

## Graphical Abstract

karlin@jhu.edu, edward.solomon@stanford.edu.

Conflict of interest

The authors declare no conflict of interest.

Supporting information for this article is given via a link at the end of the document.

Institute and/or researcher Twitter usernames: @KarlinLab

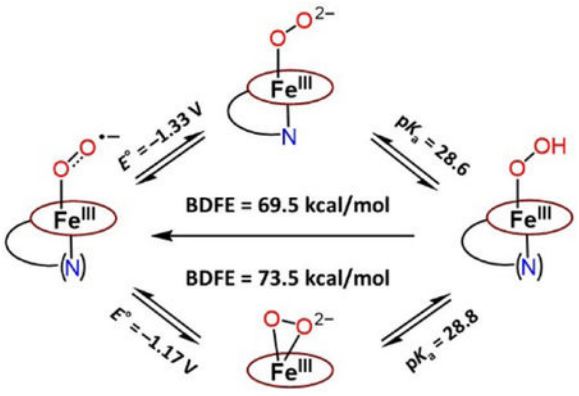


**Keywords**

end-on peroxide; bond dissociation free energy; BDFE; hydrogen atom transfer; square scheme; thermodynamic parameters

## Introduction

Heme-containing enzymes show diverse biological functions such as substrate monooxygenation, oxygen reduction in the respiratory chain, nitric oxide synthesis, oxygen storage and delivery, electron transfer, and $H_2O_2$ activation and dismutation.[1] Heme enzyme active sites contain a proximal ligand; cytochrome P450s (CYP450s) as well as NO synthase and chloroperoxidase utilize a cysteinate residue, whereas other peroxidases include a histidyl proximal ligand and catalases possess a tyrosinate ligand. The identity and nature of the axial ligand contributes to or defines spectroscopic properties, coordination, iron reduction potentials and thus the reactivity. These proximal ligand donors contribute the so-called “push effect”, due to their electron donation.[1] In particular, the “push effect” of the anionic thiolate ligand in CYP450s leads to a much more negative $Fe^{III/II}$ reduction potential[2] and helps effect the heterolytic O—O bond cleavage of a hydroperoxide species, forming Compound I (Cmpd I, $(P^{\bullet+})Fe^{IV}=O$) as the reactive species which hydroxylates substrates.[1]

CYP450 monooxygenases transfer one atom of $O_2$ to a substrate, giving hydroxylated, epoxidized, or sulfoxidized products.[1] The reaction cycle involves formation of heme $Fe^{III}$—superoxide (the initial $Fe^{II}/O_2$ adduct), with subsequent transformation to $Fe^{III}$—peroxide and $Fe^{III}$—hydroperoxide intermediates prior to O—O cleavage to give Cmpd I.[1,4]

For these three initial $Fe^{III}$ CYP450 intermediates, radiolytic cryoreduction/spectroscopic studies and theoretical calculations lead to the conclusion that all have an end-on binding geometry, with $Fe^{III}$-coordination only to the $O_2$-derived proximal oxygen atom.[5] Synthetic bioinorganic groups have been interested in the characterization of model compounds for the superoxide, peroxide, or hydroperoxide intermediates, as relevant to $O_2$ or $H_2O_2$ activating heme enzymes. There are many known ferric heme superoxide[6] and hydroperoxide synthetic compounds.[3,6g,6i,6j,7] Valentine and co-workers[8] originally synthesized and

characterized a series of ferric heme peroxides possessing a side-on bound $O_2^{2-}$ ligand ($\eta^2$, with both peroxide O-atoms equivalently bound to $Fe^{III}$). To date, there has been only one report of an end-on ($\eta^1$) bound low-spin peroxide synthetic complex, $[(P)Fe^{III}—(\eta^1{:}O_2^{2-})]^-$ (P possesses an internal imidazolyl axial ligand), that by Naruta and co-workers.[6g] Recently, we[3,6d] reported on an end-on ferric heme superoxide, a corresponding hydroperoxide species, and the related ferric heme peroxide, where the $O_2$-derived $O_2^{2-}$ ligand is side-on bound (Figure 1, upper right); the chemistry was carried out in tetrahydrofuran (THF), which serves as an axial base ligand. In that work,[3] thermodynamic parameters, the $[(F_8)Fe^{III}—(O_2^{\bullet-})]$ (***S***) reduction potential and $[(F_8)Fe^{III}—(OOH)]$ (***HP***) p$K_a$, led to the determination of the ferric heme hydroperoxide BDFE to be 73.5 kcal/mol.

Herein, the newly generated end-on low-spin peroxide, $[(P^{Im})Fe^{III}—(O_2^{2-})]^-$ (**$P^{Im}$-*P***), and its subsequent conversion to hydroperoxide species, $[(P^{Im})Fe^{III}—(OOH)]$ (**$P^{Im}$-*HP***) are described. The $P^{Im}$ porphyrinate possesses an appended axial base strongly donating imidazolyl group (Figure 1), in partial analogy to the strongly donating cysteinate base in CYP450s; $Fe^{III}$ is bound to only one oxygen atom of the peroxide moiety. Also, a reduction potential for the $[(P^{Im})Fe^{III}—(O_2^{\bullet-})]$ (**$P^{Im}$-*S***)/ $[(P^{Im})Fe^{III}—(O_2^{2-})]^-$ (**$P^{Im}$-*P***) couple and a p$K_a$ for the $[(P^{Im})Fe^{III}—(OOH)]$ (**$P^{Im}$-*HP***) acid-base pair are established here. These thermodynamic parameters and use of the Bordwell relationship square scheme (Figure 1) allow the determination of OO—H bond dissociation free energy (BDFE) for **$P^{Im}$-*HP***. We compare and contrast our thermodynamic findings and HAT reactivity with substrates to those obtained with a previously studied system employing the $F_8$ porphyrinate (Figure 1).

## Results and Discussion

The ferric heme superoxide $[(P^{Im})Fe^{III}—(O_2^{\bullet-})]$ (**$P^{Im}$-*S***) generated by bubbling $O_2$ to a solution of $[(P^{Im})Fe^{II}]$ (Figure 1), was previously characterized ($\nu_{O—O}$, 1180 ($\Delta^{18}O_2$, −56) $cm^{-1}$; $\nu_{Fe\text{-}O}$, 575 ($\Delta^{18}O_2$, −23) $cm^{-1}$).[6h,9] Addition of cobaltocene ($CoCp_2$) to **$P^{Im}$-*S*** at −80 ℃ in THF results in the formation of the ferric heme peroxide complex $[(P^{Im})Fe^{III}—(O_2^{2-})]^-$ (**$P^{Im}$-*P***); UV-vis spectral shifts occurring are 423 to 424 nm (Soret) and 532 to 535, 567 nm (Figure 2A). These product electronic absorption spectra are very similar to those of Naruta's end-on low-spin ferric heme peroxide, as mentioned the first of its kind.[6g] The UV-vis features of **$P^{Im}$-*P*** and Naruta's analog exhibit higher energy Soret $\lambda_{max}$ values than the side-on bound ferric heme peroxides (also lacking a trans axial base ligand), as in $[(F_8)Fe^{III}—(\eta^2{:}O_2^{2-})]^-$ (Figure 1, upper right).[3,6d,6f,8] The low-spin end-on formulation is confirmed by the EPR spectra which display signals at $g$ = 2.25, 2.14, and 1.95 (Figure 2A), matching Naruta's analog,[6g] as well as for those end-on ferric peroxide obtained by cryoreduction methods in heme enzymes.[5] Such EPR signatures also are distinct from side-on heme peroxide intermediates which are intermediate spin species, $g$ = 4.2 (S = 3/2).[3,6d,6f,8]

Further, $[(P^{Im})Fe^{III}—(O_2^{2-})]^-$ (**$P^{Im}$-*P***) was characterized using rR spectroscopy. Two isotopic sensitive bands were observed, at 810 ($\Delta^{18}O_2$ = −34) $cm^{-1}$ and 578 ($\Delta^{18}O_2$ = −26) $cm^{-1}$ corresponding to the $\nu_{O—O}$ and $\nu_{Fe—O}$ stretches, respectively (Figure 2B). This latter stretching frequency value matches the expected value ($\Delta_{Fe\text{-}O,calc}$ ($^{16}O_2/^{18}O_2$) = −26 $cm^{-1}$) using the harmonic oscillator approximation. The magnitude of the isotope shift for $\nu_{O—O}$ is

smaller than the calculated value ($\Delta_{O\text{-}O,calc}$ ($^{16}O_2/^{18}O_2$) = −46 $cm^{-1}$); however, the same trend is found for Naruta's complex [(P)$Fe^{III}$—($\eta^1$:$O_2^{2-}$)]$^-$ ($\nu_{O—O}$, 808 ($\Delta^{18}O_2$, −37) $cm^{-1}$; $\nu_{Fe\text{-}O}$, 585 ($\Delta^{18}O_2$, −25) $cm^{-1}$).[6g] It is notable that $\nu_{Fe—O}$ in [($P^{Im}$)$Fe^{III}$—($\eta^1$:$O_2^{2-}$)]$^-$ (**$P^{Im}$-*P***) is much larger than that found for the side-on peroxide species which has no internally appended axial base imidazolyl, [($F_8$)$Fe^{III}$—($\eta^2$:$O_2^{2-}$)]$^-$ (Figure 1, upper right; $\nu_{O—O}$, 806 ($\Delta^{18}O_2$, −46) $cm^{-1}$; $\nu_{Fe\text{-}O}$, 466 ($\Delta^{18}O_2$, −19) $cm^{-1}$).[3] The increased Fe—O stretching frequency is likely a result of both the monodentate coordination and the σ-symmetry $O_2$ donation into the fully unoccupied low-spin Fe $d_{z2}$ orbital which is stronger than the π-symmetry donation into the half-occupied Fe $d_{xz}/d_{yz}$ orbital of the side-on peroxide complex. These effects would strengthen the Fe—O bond of **$P^{Im}$-*P***, and favor the end-on binding mode, giving a low-spin six-coordinate species [($P^{Im}$)$Fe^{III}$—($\eta^1$:$O_2^{2-}$)]$^-$ (**$P^{Im}$-*P***).

When excess triflic acid (HOTf) is added to [($P^{Im}$)$Fe^{III}$—($O_2^{2-}$)]$^-$ (**$P^{Im}$-*P***), Fe—O bond cleavage occurs, releasing $H_2O_2$ (89 % yield; horseradish peroxidase assay, see Figure S1), corroborating the complex's peroxide formulation. **$P^{Im}$-*P*** is singly protonated by adding 1 equiv of 2,6-lutidinium triflate [($LutH^+$)](OTf) at −80 ℃ in THF, giving [($P^{Im}$)$Fe^{III}$—(OOH)] (**$P^{Im}$-*HP***) with absorptions at 423 and 533 nm (Figure 3A). EPR spectra of **$P^{Im}$-*HP*** confirm an end-on low-spin ferric heme hydroperoxide structure ($g$ = 2.25, 2.14, and 1.95) as shown in Figure 3B. These values correspond closely to those already known for synthetically derived end-on low-spin hydroperoxide complexes[3,6f,6g,6i,6j,7a,7b] as well as for ferric heme hydroperoxides generated within hemoglobin and myoglobin.[10a,b] A high yield of $H_2O_2$ (90.1 %) is also obtained when **$P^{Im}$-*HP*** is acidified using HOTf (see Figure S1). Further, we performed rR spectroscopy; while only noisy spectra could be obtained (Figure S2), $\nu_{O—O}$ (808 ($\Delta^{18}O_2$, −48) $cm^{-1}$) and $\nu_{Fe—O}$ (579 ($\Delta^{18}O_2$, −36) $cm^{-1}$) resonances could be well discerned. These parameters, for **$P^{Im}$-*HP***, are quite similar to those for the other synthetic or protein low-spin ferric heme hydroperoxide complexes (vide supra).[3,6g,7c,10]

We find [($P^{Im}$)$Fe^{III}$—($O_2^{\bullet-}$)] (**$P^{Im}$-*S***) and [($P^{Im}$)$Fe^{III}$—($O_2^{2-}$)]$^-$ (**$P^{Im}$-*P***) are interconvertible (Figure 1) using redox reagents. Addition of a ferrocenium reagent ($Fc^+$; $E_{1/2}$ = 0 V vs $Fc^{+/0}$) to a solution of **$P^{Im}$-*P*** leads to the reappearance of the optical bands (423 and 532 nm) associated with **$P^{Im}$-*S*** (Figure S3). This result is supported by the diamagnetic behaviour (i.e., EPR silent; 10 K, THF) of the resulting **$P^{Im}$-*S*** solution. The further addition of $CoCp_2$ leads to re-reduction giving the peroxide species **$P^{Im}$-*P*** (Figure S4).

Interestingly, titration of [($P^{Im}$)$Fe^{III}$—($O_2^{\bullet-}$)] (**$P^{Im}$-*S***) with aliquots of $CoCp_2$ ($E_{1/2}$ = −1.33 V vs $Fc^{+/0}$ in THF)[11] at −80 ℃ in THF gives equilibrium mixtures; UV-vis monitoring (at either 423 or 567 nm) (Figure 4A, Table S1, Figure S5), allowed determination of $K_{eq}$ for each aliquot added. From these results and utilizing the Nernst equation, the reduction potential for the couple, [($P^{Im}$)$Fe^{III}$—($O_2^{\bullet-}$)] (**$P^{Im}$-*S***)/[($P^{Im}$)$Fe^{III}$—($O_2^{2-}$)]$^-$ (**$P^{Im}$-*P***) is calculated to be −1.33 V ± 0.01 V vs $Fc^{+/0}$. This value is more negative by ~160 mV than that reported for [($F_8$)$Fe^{III}$—($O_2^{\bullet-}$)] (−1.17 V vs $Fc^{+/0}$) (Figure S6) which has no internally appended axial base in the porphyrinate complex.[3] Consistent with this finding is the observation that in order to fully reduce [($F_8$)$Fe^{III}$—($O_2^{\bullet-}$)] to its peroxide analogue, one equiv $CoCp_2$ was used, while multiple equiv of $CoCp_2$ are required to fully reduce the

presently described superoxide complex **$P^{Im}$-*S***. These findings suggest a “push effect” due to the axial imidazolyl ligand which is covalently appended to the heme of $P^{Im}$ iron-porphyrinate complexes.

Dey and co-workers[2] reported the reduction potentials of iron-porphyrinate complexes ($Fe^{III/II}$) which have thiolate and imidazolyl linkers bound to the iron center of porphyrinate complexes. A thiolate ligated porphyrin complex shows 500 mV more negative $Fe^{III/II}$ reduction potential compared to an imidazolyl ligated porphyrinate analogue; the thiolate is a much better donor than imidazolyl. Never-the-less, in our case the greater charge donation by an axial imidazolyl ligand in $P^{Im}$ reduces the reduction potential of [($P^{Im}$)$Fe^{III}$—($O_2^{\bullet -}$)] (**$P^{Im}$-*S***) in comparison with that of [($F_8$)$Fe^{III}$—($O_2^{\bullet -}$)].

To complete the thermodynamic square scheme analysis (Figure 1),[12] the p$K_a$ value of ferric heme hydroperoxide [($P^{Im}$)$Fe^{III}$—(OOH)] (**$P^{Im}$-*HP***) was evaluated at −80 ℃ in THF. Full deprotonation of **$P^{Im}$-*HP*** was accomplished by spectral titration using the derivatized phosphazene base $EtP_2$(dma) (see Table S2 for the chemical structure; conjugate base p$K_a$ = 28.1; THF solvent, RT).[13] The concentrations of each species (**$P^{Im}$-*P***, **$P^{Im}$-*HP***, $EtP_2$(dma), and $EtP_2(dma)H^+$) were evaluated by examination of the observed absorbance at either 423 or 567 nm in the UV-vis spectra (Figure 4B, Table S2, Figure S7). Such titration experiments lead to the establishment of $K_{eq}$ constants for the protonation of **$P^{Im}$-*P*** to give **$P^{Im}$-*HP***, allowing the calculation of the p$K_a$ of the ferric heme hydroperoxide to be 28.6 ± 0.5 (−80 °C, THF). The reversibility of acid-base reaction was further demonstrated by adding [(Lut$H^+$)](OTf) to the solution generated in this titration, which gives back **$P^{Im}$-*HP***, (Figure S8).

This allows the completion of the thermodynamic square scheme for electron and proton transfer reactions (Figure 1) using the presently determined thermodynamic parameters, *E*°’ (−1.33 V vs. $Fc^{+/0}$, vide supra) and p$K_a$ (28.6, vide supra), and determination of the BDFE of the OO—H in the ferric heme hydroperoxide complex [($P^{Im}$)$Fe^{III}$—(OOH)] (**$P^{Im}$-*HP***). According to eq. 1 (Bordwell relationship, $C_G$ stands for the $H^+/H^{\bullet}$ standard reduction potential in a particular solvent),[12] where $C_G$ = 61 kcal/mol in THF, the **$P^{Im}$-*HP*** BDFE is calculated to be 69.5 kcal/mol (eq. 2).

$$\mathbf{BDFE} = 1.37(\mathrm{p}K_a) + 23.06E^{o} + C_{G,\,solv} \quad (1)$$

$$\mathbf{BDFE}_{OO-H} = 1.37(28.6) + 23.06(-1.33) + 61 = \mathbf{69.5\,kcal/mol} \quad (2)$$

Our own previous report is the only other experimental evaluation of the thermodyanmics and use of the square shcme as applied to ferric heme superoxide, peroxide (Figure 1, upper right) and hydroperoxide relatives, i.e., for the $F_8$ heme containing superoxide, (side-on) peroxide and hydroperoxide, [($F_8$)$Fe^{III}$—(OOH]] $BDFE_{OO—H}$ = 73.5 kcal/mol.[3] Our OO—H BDFE value presented here with $P^{Im}$ is shown to be ~ 4 kcal/mol less, and the difference resides primarily in the variation in the superoxide/peroxide redox couple (Figure 5).

The p$K_a$ values for [($F_8$)$Fe^{III}$—(OOH)] vs [($P^{Im}$)$Fe^{III}$—(OOH)] (**$P^{Im}$-*HP***) are essentially identical,[14] but the $E°'$ reduction potential is measurably more negative for the (**$P^{Im}$-*S***) / (**$P^{Im}$-*P***) couple (Figure 5). This makes chemical sense as the $P^{Im}$ system possesses the strong imidazolyl axial base ligand donor, that not present in the $F_8$ heme system. Also, the dissimilarity of BDFE values ([($P^{Im}$)$Fe^{III}$—(OOH)] $BDFE_{OO—H}$ = 69.5 kcal/mol and [($F_8$)$Fe^{III}$—(OOH)] $BDFE_{OO—H}$ = 73.5 kcal/mol) is supported by their hydrogen atom transfer (HAT) reactivities toward H atom donors (vide infra). As we noted previously[3] our BDFE results are also roughly in accord with computationally derived ferric heme hydroperoxides (those modeling proteins), where a proximal ligand is either an imidazolyl or —SH group, BDEs (64–66 kcal/mol).[15]

HAT reactivity (shown in the diagonal of Figure 1) studies were performed with [($P^{Im}$)$Fe^{III}$—($O_2^{\bullet-}$)] (**$P^{Im}$-*S***) toward external substrates to support our experimentally determined BDFE value. Addition of an excess of substrates such as 9,10-dihydroanthracene (76 kcal/mol in DMSO)[12] and xanthene (72.2 kcal/mol in THF)[13] to the solutions of **$P^{Im}$-*S*** at −80 ℃ in THF led to no reaction. These observations are consistent with our BDFE determination of 69.5 kcal/mol for [($P^{Im}$)$Fe^{III}$—(OOH)] (**$P^{Im}$-*HP***). In contrast, TEMPO-H (66.5 (THF), 72.6 (aq. buffer), and 69.6 (benzene) kcal/mol)[13,16] does react with complex **$P^{Im}$-*S***. The final spectra (UV-vis and EPR; Figure 6A, Figure S9 and S10) reveal a high yield of TEMPO•, while **$P^{Im}$-*HP*** seems to only form in small amounts (~20% yield), probably due to side-reactions. The results support the conclusion that an initial H-atom abstraction from TEMPO-H to give **$P^{Im}$-*HP*** occurred. Based on these reactivity studies, the BDFE of **$P^{Im}$-*HP*** can be bracketed to be, 66.5 < $BDFE_{OO—H}$ < 72 kcal/mol, which is consistent with our experimentally determined BDFE value, 69.5 kcal/mol.

As we previously showed that [($F_8$)$Fe^{III}$—($O_2^{\bullet-}$)] (***S***) reacts with TEMPO-H to cleanly give the TEMPO• and corresponding hydroperoxide complex [($F_8$)$Fe^{III}$—(OOH)] (***HP***), we now see that ***S*** and [($P^{Im}$)$Fe^{III}$—($O_2^{\bullet-}$)] (**$P^{Im}$-*S***) reactions toward TEMPO-H are comparable. Thus, we sought to find a different substrate that might differentiate between the oxidizing capabilities of the two superoxide complexes, which is what we have found here based on our thermodynamic parameter analysis. The superoxide complex ***S*** should be a somewhat stronger oxidant for HAT chemistry as based on our finding of the ~ 4 kcal/mol difference in ***HP*** versus **$P^{Im}$-*HP*** complexes' BDFEs (vide supra).

Thus, we turned to the use of the hydroxylamine substrate ABNO-H (9-azabicyclo[3.3.1]nonane-*N*-hydroxide, BDFE = 76.0 (aq. buffer) and 76.2 (benzene) kcal/mol)[16] whose BDFE value is in the range 3.4-to-6.6 kcal/mol higher than that of TEMPO-H. As summarized in Figure 6, there was no reaction between [($P^{Im}$)$Fe^{III}$—($O_2^{\bullet-}$)] (**$P^{Im}$-*S***) and ABNO-H (Figure 6A and Figure S11), while spectroscopic monitoring (UV-vis and EPR) of the corresonding [($F_8$)$Fe^{III}$—($O_2^{\bullet-}$)] (***S***) plus ABNO-H reaction (Figure 6B and Figure S12) revealed both the generation of the organic radical product (ABNO•) along with the formation of the low-spin end-on hydroperoxide species, ***HP*** (See Figure S12 for further details). The HAT reaction of ABNO-H with **$P^{Im}$-*S*** is thermodynamically uphill. In contrast, the oxidizing ability of ***S*** via HAT from ABNO-H is favored. ABNO-H is a borderline substrate which enables us to discern the clear difference in the reactivities between **$P^{Im}$-*S***

and ***S***; the results are fully consistent with our findings of heme-hydroperoxide OO—H BDFE's via thermodynamic analyses, here and previously.[3]

## Conclusion

In conclusion, using the $P^{Im}$ iron-porphyrinate which includes an imidazolyl moiety appended to the periphery of a fluorinated tetraphenylporphyrin, we here generated a new (only the second one known) end-on low-spin ferric heme peroxide $[(P^{Im})Fe^{III}—(O_2^{2-})]^-$ (**$P^{Im}$-*P***) and also a hydroperoxide $[(P^{Im})Fe^{III}—(OOH)]$ (**$P^{Im}$-*HP***) species which are relevant to the catalytic cycle of CYP450s and many other heme enzymes which activate $O_2$ or $H_2O_2$. The end-on peroxide binding mode with the $P^{Im}$ heme contrasts with that of the $F_8$ heme (without the appended axial imidazolyl ligand) which forms a side-on peroxide species. The reversibility of the $[(P^{Im})Fe^{III}—(O_2^{\bullet-})]$ (**$P^{Im}$-*S***)/ $[(P^{Im})Fe^{III}—(O_2^{2-})]^-$ (**$P^{Im}$-*P***) redox process and the $[(P^{Im})Fe^{III}—(O_2^{2-})]^-$ (**$P^{Im}$-*P***)/ $[(P^{Im})Fe^{III}—(OOH)]$ (**$P^{Im}$-*HP***) acid-base equilibrium allowed for the calculation of reduction potential and p$K_a$, respectively. With the measured thermodynamic parameters, the ferric heme OO—H BDFE was determined to be 69.5 kcal/mol, contrasting with the value of 73.5 kcal/mol found for $[(F_8)Fe^{III}—(OOH)]$ (***HP***).

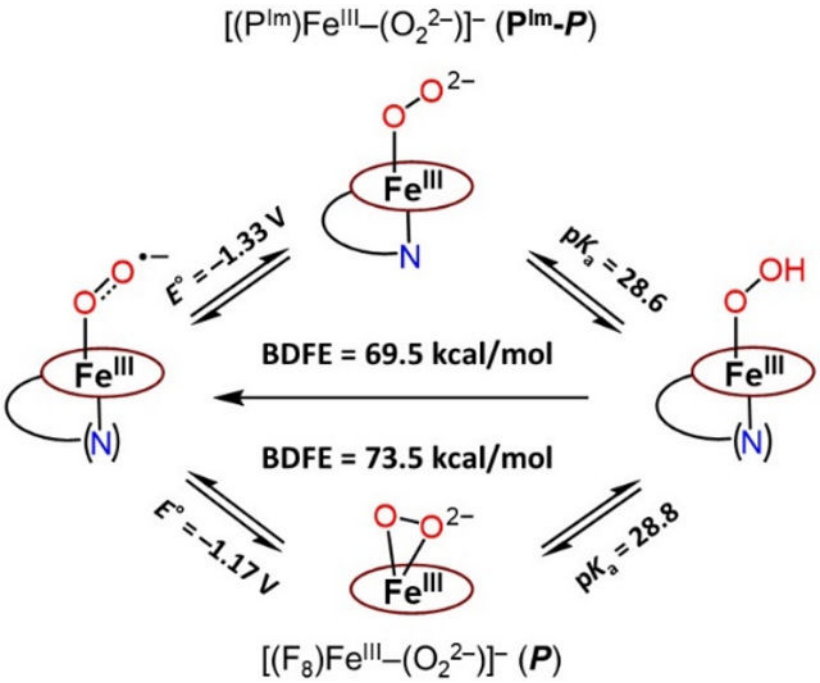


This difference is a result of the existence of the appended axial imidazolyl ligand in the $P^{Im}$ system. Its "push effect" appears to contribute significantly to the lower reduction potential found for (**$P^{Im}$-*S***)/(**$P^{Im}$-*P***) compared to that measured for the (***S***)/(***P***) couple with $F_8$-heme. Confirmation of our thermodynamically derived parameters comes from comparison of the $[(P^{Im})Fe^{III}—(O_2^{\bullet-})]$ (**$P^{Im}$-*S***) versus $[(F_8)Fe^{III}—(O_2^{\bullet-})]$ (***S***) reactivity results employing the hydroxylamine substrates TEMPO-H and/or ABNO-H. Future studies will explore further

similar thermodynamic relationships to determine how ligand effects may control such properties and chemical reactivity.

## Supplementary Material

Refer to Web version on PubMed Central for supplementary material.

## Acknowledgements

This research was supported by the U.S. National Institutes of Health (GM60353 to K.D.K. and GM040392 to E.I.S.).

## References

[1]. a)Sono M, Roach MP, Coulter ED, Dawson JH, Chem. Rev 1996, 96, 2841–2887; [PubMed: 11848843] b)Denisov IG, Makris TM, Sligar SG, Schlichting I, Chem. Rev 2005, 105, 2253–2277; [PubMed: 15941214] c)Ortiz de Montellano PR, Chem. Rev 2010, 110, 932–948; [PubMed: 19769330] d)Huang X, Groves JT, Chem. Rev 2018, 118, 2491–2553; [PubMed: 29286645] e)Adam SM, Wijeratne GB, Rogler PJ, Diaz DE, Quist DA, Liu JJ, Karlin KD, Chem. Rev 2018, 118, 10840–11022. [PubMed: 30372042]

[2]. Das PK, Chatterjee S, Samanta S, Dey A, Inorg. Chem 2012, 51, 10704–10714. [PubMed: 23013308]

[3]. Kim H, Rogler PJ, Sharma SK, Schaefer AW, Solomon EI, Karlin KD, J . Am. Chem. Soc 2020, 142, 3104–3116. [PubMed: 31913628]

[4]. Dubey KD, Shaik S, Acc. Chem. Res 2019, 52, 389–399. [PubMed: 30633519]

[5]. a)Davydov R, Macdonald IDG, Makris TM, Sligar SG, Hoffman BM, J. Am. Chem. Soc 1999, 121, 10654–10655;b)Davydov R, Makris TM, Kofman V, Werst DE, Sligar SG, Hoffman BM, J. Am. Chem. Soc 2001, 123, 1403–1415; [PubMed: 11456714] c)Davydov R, Satterlee JD, Fujii H, Sauer-Masarwa A, Busch DH, Hoffman BM, J. Am. Chem. Soc 2003, 125, 16340–16346; [PubMed: 14692776] d)Garcia-Serres R, Davydov RM, Matsui T, Ikeda-Saito M, Hoffman BM, Huynh BH, J. Am. Chem. Soc 2007, 129, 1402–1412; [PubMed: 17263425] e)Shaik S, Cohen S, Wang Y, Chen H, Kumar D, Thiel W, Chem. Rev. 2010, 110, 949–1017. [PubMed: 19813749]

[6]. a)Collman JP, Gagnet RR, Christopher A, Robinson WT, Proc. Natl. Acad. Sci. U. S. A 1974, 71, 1326–1329; [PubMed: 4524640] b)Momenteau M, Reed CA, Chem. Rev 1994, 94, 659–698;c)Collman JP, Sunderland CJ, Berg KE, Vance MA, Solomon EI, J. Am. Chem. Soc 2003, 125, 6648–6649; [PubMed: 12769571] d)Chufan EE, Karlin KD, J. Am. Chem. Soc. 2003, 125, 16160–16161; [PubMed: 14692736] e)Liu J-G, Naruta Y, Tani F, Angew. Chem. Int. Ed 2005, 44, 1836–1840;Angew. Chem 2005, 117, 1870–1874;f)Liu J-G, Ohta T, Yamaguchi S, Ogura T, Sakamoto S, Maeda Y, Naruta Y, Angew. Chem. Int. Ed. Engl 2009, 48, 9262–9267; [PubMed: 19882613] Angew. Chem 2009, 121, 9426–9431;g)Liu J-G, Shimizu Y, Ohta T, Naruta Y, J. Am. Chem. Soc 2010, 132, 3672–3673; [PubMed: 20196593] h)Li Y, Sharma SK, Karlin KD, Polyhedron 2013, 58, 190–196;i)Nagaraju P, Ohta T, Liu J-G, Ogura T, Naruta Y, Chem. Commun 2016, 52, 7213–7216;j)Singha A, Dey A, Chem. Commun 2019, 55, 5591–5594;k)Kim H, Sharma SK, Schaefer AW, Solomon EI, Karlin KD, Inorg. Chem 2019, 58, 15423–15432. [PubMed: 31657921]

[7]. a)Tajima K, Oka S, Edo T, Miyake S, Mano H, Mukai K, Sakurai H, Ishizu K, J. Chem. Soc., Chem. Commun, 1995, 1507–1508;b)Oliveira R, Zouari W, Herrero C, Banse F, Schöllhorn B, Fave C, Anxolabéhère-Mallart E, Inorg. Chem 2016, 55, 12204–12210; [PubMed: 27934428] c)Sengupta K, Chatterjee S, Samanta S, Dey A, Proc. Natl. Acad. Sci. U. S. A 2013, 110, 8431–8436. [PubMed: 23650367]

[8]. a)McCandlish E, Miksztal AR, Nappa M, Spreger AQ, Valentine JS, J. Am. Chem. Soc 1980, 102, 4268–4271;b)Selke M, Sisemore MF, Valentine JS, J. Am. Chem. Soc 1996, 118, 2008–2012;c)Wertz DL, Valentine JS, Struct. Bonding (Berlin) 2000, 97, 37–60.

[9]. Sharma SK, Schaefer AW, Lim H, Matsumura H, Moënne-Loccoz P, Hedman B, Hodgson KO, Solomon EI, Karlin KD, J. Am. Chem. Soc 2017, 139, 17421–17430. [PubMed: 29091732]

[10]. a)Mak PJ, Denisov IG, Victoria D, Makris TM, Deng T, Sligar SG, Kincaid JR, J. Am. Chem. Soc 2007, 129, 6382–6383; [PubMed: 17461587] b)Denisov IG, Mak PJ, Makris TM, Sligar SG, Kincaid JR, J. Phys. Chem. A 2008, 112, 13172–13179; [PubMed: 18630867] c)Davydov RM, Yoshida T, Ikeda-Saito M, Hoffman BM, J. Am. Chem. Soc 1999, 121, 10656–10657;d)Ibrahim M, Denisov IG, Makris TM, Kincaid JR, Sligar SG, J. Am. Chem. Soc 2003, 125, 13714–13718. [PubMed: 14599210]

[11]. Yandulov DV, Schrock RR, Inorg. Chem 2005, 44, 1103–1117. [PubMed: 15859292]

[12]. Warren JJ, Tronic TA, Mayer JM, Chem. Rev 2010, 110, 6961–7001. [PubMed: 20925411]

[13]. Quist DA, Ehudin MA, Schaefer AW, Schneider GL, Solomon EI, Karlin KD, J. Am. Chem. Soc 2019, 141, 12682–12696. [PubMed: 31299154]

[14]. We are somewhat surprised by the observation that $\mathbf{P^{Im}}$-***HP*** and ***HP*** have very similar p$K_a$ values. However, explanations for this seem to not now exist the literature and further detailed experimental and computational investigations are required. To compare hydroperoxide p$K_a$'s is not straightforward since the conjugate base peroxide complexes $\mathbf{P^{Im}}$-***P*** and ***P*** have different structures, end-on vs. side-on.

[15]. Chung LW, Li X, Hirao H, Morokuma K, J. Am. Chem. Soc 2011, 133, 20076–20079. [PubMed: 22047171]

[16]. Gerken JB, Pang YQ, Lauber MB, Stahl SS, J. Org. Chem 2018, 83, 7323–7330. [PubMed: 29182282]

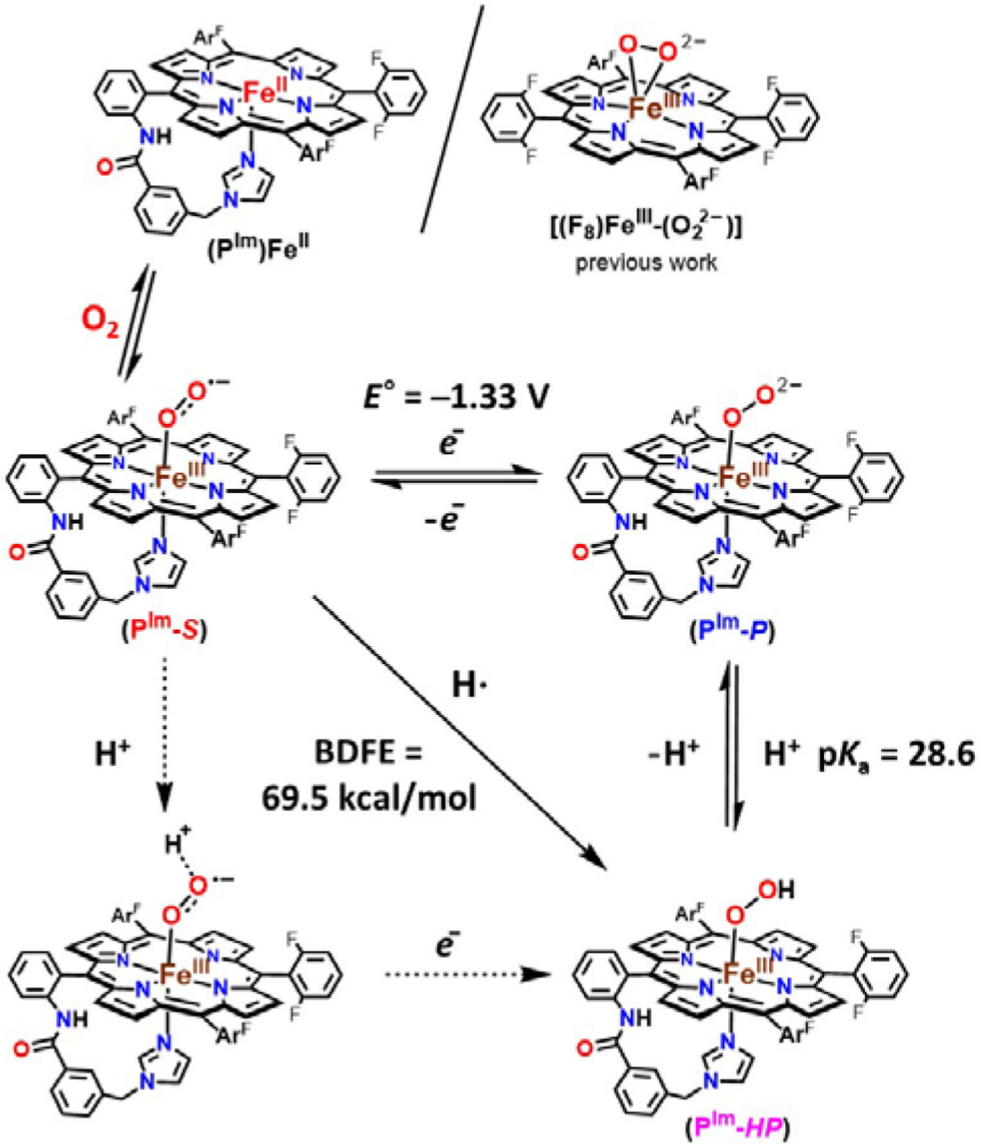


**Figure 1.**

Stepwise generation of superoxide, peroxide, and hydroperoxide heme analogues and relevant thermodynamic square scheme ($E°$ as determined vs $Fc^{+/0}$ and p$K_a$) and OO—H BDFE of ferric heme hydroperoxide. $Ar^F$ = 2,6-difluorophenyl group. Upper right: the previously studied ferric heme peroxide $[(F_8)Fe^{III}—(\eta^2{:}O_2{}^{2-})]^-$.[3]

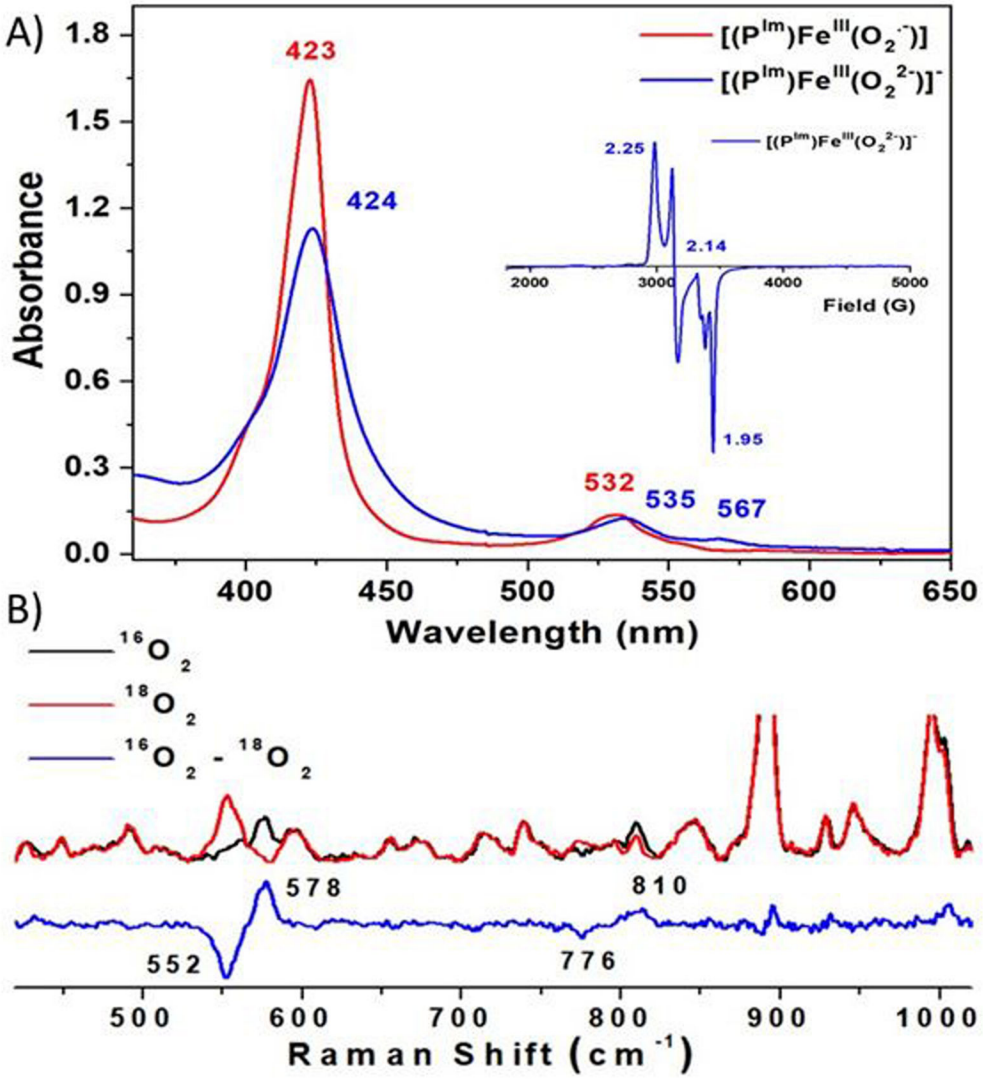


**Figure 2.**

(A) Electronic absorption spectra of [($P^{Im}$)$Fe^{III}$—($O_2^{\bullet-}$)] (**$P^{Im}$-*S***) (red) to [($P^{Im}$)$Fe^{III}$—($O_2^{2-}$)]$^-$ (**$P^{Im}$-*P***) (blue) at −80 ℃ in THF. Inset: Frozen THF solution EPR (10 K) spectrum of **$P^{Im}$-*P***. The small feature ($g$ = 1.99) corresponds to an excess of cobaltocene.[6d] (B) Resonance Raman spectra of [($P^{Im}$)$Fe^{III}$—($O_2^{2-}$)]$^-$ (**$P^{Im}$-*P***) in frozen THF obtained at 77 K with 413 nm excitation. The $^{16}O_2$—$^{18}O_2$ difference spectrum is shown in blue.

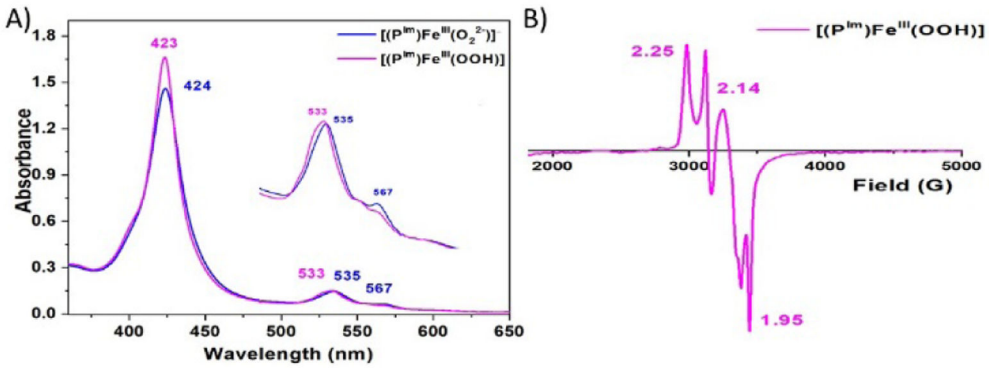


**Figure 3.**

(A) UV–vis spectra illustrating the conversion of $[(P^{Im})Fe^{III}—(O_2^{2-})]^-$ (**$P^{Im}$-*P***) to $[(P^{Im})Fe^{III}—(OOH)]$ (**$P^{Im}$-*HP***) by addition of $[(LutH^+)](OTf)$ at −80 ℃ in THF. (B) Low-spin EPR spectrum (10 K) of **$P^{Im}$-*HP***. Note that there is $g = 1.99$ signal from excess of cobaltocene used for generation of the peroxide complex. An extra signal at g > 2.00 (compared to the EPR spectrum shown in Figure 2) is attributed to an unknown impurity.

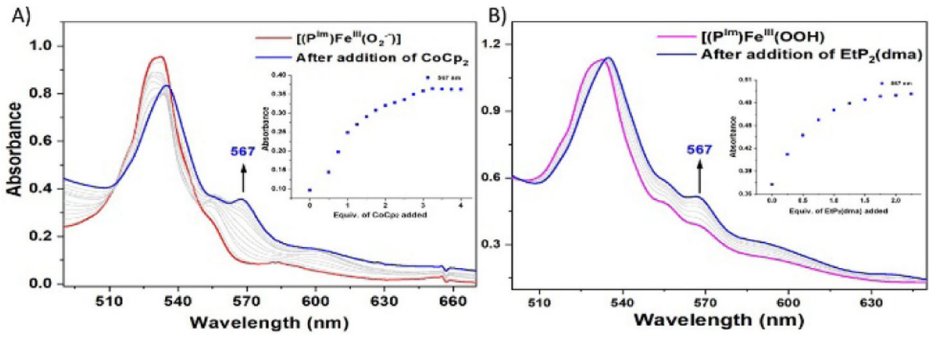


**Figure 4.**

UV-vis spectroscopic monitoring of the incremental addition of (A) $CoCp_2$ to a solution of [($P^{Im}$)$Fe^{III}$—($O_2^{\bullet-}$)] (**$P^{Im}$-*S***) (red). Inset: monitoring of the absorbance at 567 nm (blue). (B) $EtP_2$(dma) addition to a solution of [($P^{Im}$)$Fe^{III}$—(OOH)] (**$P^{Im}$-*HP***) (pink). Inset: monitoring of the absorbance at 567 nm (blue).

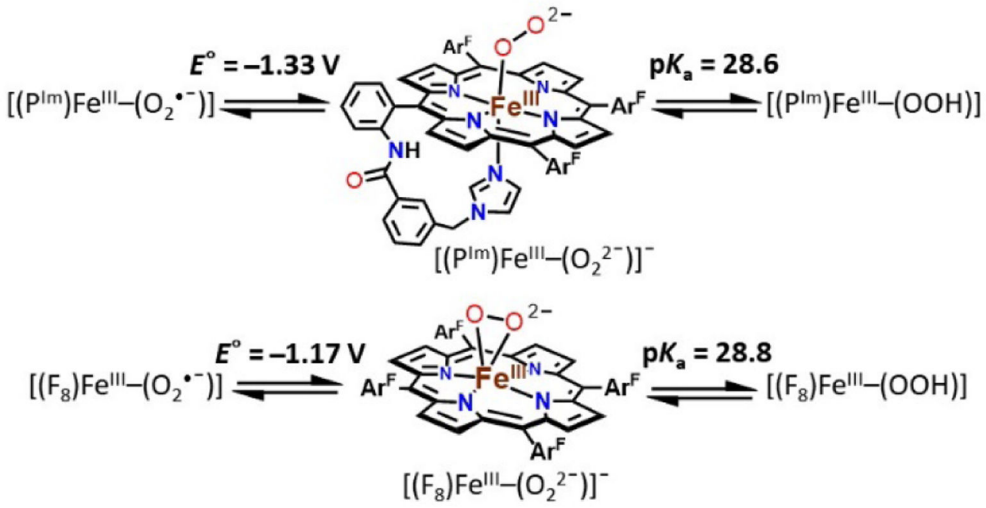


**Figure 5.**

Comparison of $P^{Im}$ and $F_8$ iron-porphyrinate complex for thermodynamic parameters and the geometry of peroxide species.

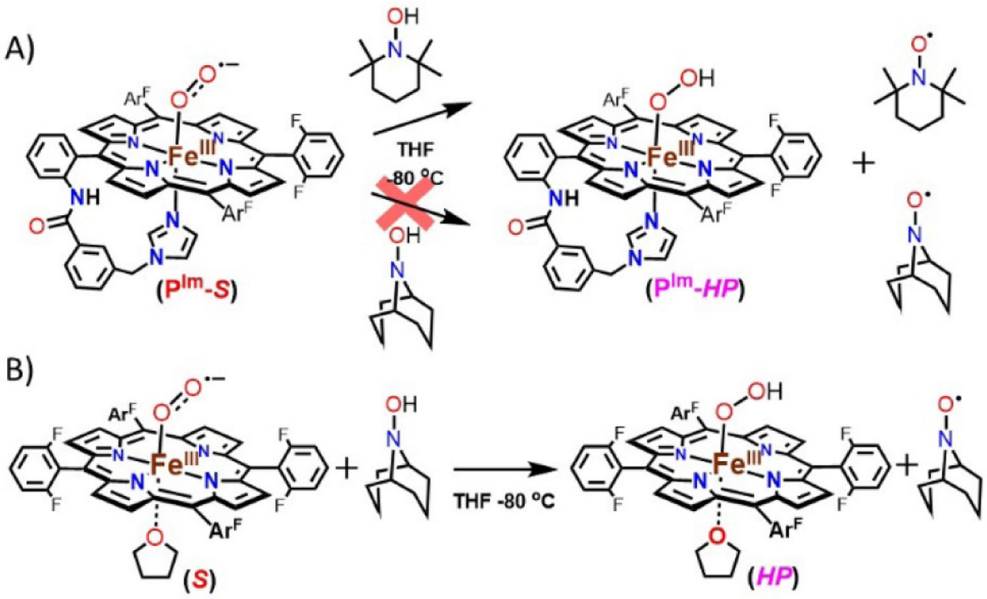


**Figure 6.**

(A) Hydrogen atom transfer (HAT) reaction by [($P^{Im}$)$Fe^{III}$—($O_2^{\bullet-}$)] (**$P^{Im}$-*S***) from TEMPO-H and ABNO-H at −80 ℃ in THF. (B) HAT from [($F_8$)$Fe^{III}$—(O2$^{\bullet-}$)] (***S***) toward ABNO-H at −80 ℃ in THF.